

This work was written as part of one of the author's official duties as an Employee of the United States Government and is therefore a work of the United States Government. In accordance with 17 U.S.C. 105, no copyright protection is available for such works under U.S. Law.

Public Domain Mark 1.0

<https://creativecommons.org/publicdomain/mark/1.0/>

Access to this work was provided by the University of Maryland, Baltimore County (UMBC) ScholarWorks@UMBC digital repository on the Maryland Shared Open Access (MD-SOAR) platform.

Please provide feedback

Please support the ScholarWorks@UMBC repository by emailing scholarworks-group@umbc.edu and telling us what having access to this work means to you and why it's important to you. Thank you.



Global effects of transmitted shock wave propagation through the Earth's inner magnetosphere: First results from 3-D hybrid kinetic modeling

A.S. Lipatov^{a,b,*}, D.G. Sibeck^c

^a GPHI UMBC/NASA GSFC, Code 673, Greenbelt, MD 20771, USA

^b Faculty of Problems of Physics and Power Engineering, Moscow Institute of Physics and Technology, Russia

^c NASA Goddard Space Flight Center, Code 674, Greenbelt, MD 20771, USA

ARTICLE INFO

Article history:

Received 16 February 2016

Received in revised form

12 May 2016

Accepted 30 May 2016

Available online 3 June 2016

Keywords:

Solar wind

Magnetosphere

Plasmasphere

Radiation belts

Ring current

Interplanetary shocks

ABSTRACT

We use a new hybrid kinetic model to simulate the response of ring current, outer radiation belt, and plasmaspheric particle populations to impulsive interplanetary shocks. Since particle distributions attending the interplanetary shock waves and in the ring current and radiation belts are non-Maxwellian, wave–particle interactions play a crucial role in energy transport within the inner magnetosphere. Finite gyroradius effects become important in mass loading the shock waves with the background plasma in the presence of higher energy ring current and radiation belt ions and electrons. Initial results show that shocks cause strong deformations in the global structure of the ring current, radiation belt, and plasmasphere. The ion velocity distribution functions at the shock front, in the ring current, and in the radiation belt help us determine energy transport through the Earth's inner magnetosphere.

© 2016 Elsevier Ltd. All rights reserved.

1. Introduction

Solar wind shocks striking the magnetosphere provide an excellent example of one fundamental mode of interaction between the solar wind and magnetosphere, just as interesting and important as magnetic field reconnection.

The Earth's inner magnetosphere presents a complex plasma system which includes several plasma structures – the ring current, outer radiation belt, plasmasphere, and inner radiation belt, as shown in Fig. 1.

Magnetohydrodynamic (MHD) models have been used to explain many of the signatures observed when shocks strike the magnetosphere. For example, previous workers have used three-dimensional MHD models (Lipatov, 1972; Van'yan and Lipatov, 1974a,b) to show that transmitted magnetosonic impulses are converted to Alfvén waves near the Dawn–Dusk plane. The Alfvén waves propagate along the geomagnetic field and initiate non-linear field line resonances. The recent MHD models already include the formation of the bow shock, magnetosheath, magnetopause. These models have been used to study magnetic field

reconnection and the effects of transmitted impulses propagating through the inner magnetosphere, e.g. pulsations, non-linear field line resonances, and electron acceleration caused by motional electric field associated with the interplanetary shocks (see Hudson et al., 1995, 2008, 2015; Elkington et al., 2002; Fujita et al., 2003a,b, 2005; Lipatov and Rankin, 2005, 2009; Samsonov et al., 2007; Kress et al., 2008; Zhu et al., 2009; Samsonov et al., 2011, 2014 and references therein). The shock waves inside the inner magnetosphere may result from the active experiments (see e.g. Winske and Gary, 2007; Winske and Cowee, 2012).

There are even multi-fluid models for the magnetosphere which might be used for this purpose. Such models were successfully used to study the consequences of ionospheric outflow (see e.g. Gloer et al., 2009; Winglee, 1998 and references therein). However, multi-fluid models do not describe the wave–particle (ion) interactions which develop when transmitted impulses pass through the ring current and radiation belts.

By their very nature such models miss crucial kinetic effects that are of great importance in the overall solar wind-magnetosphere interaction. The first 2.5-D hybrid (Omidi et al., 2013, 2014; Gutynska et al., 2015), 2.5-D hybrid-Vlasov (Kempf et al., 2015) and 3-D hybrid (Lin and Wang, 2005) models turned their attention to the structure of the quasi-perpendicular and quasi-parallel bow shocks, the ion velocity distribution dynamics and perturbations in the plasma density and magnetic field inside the plasmasheath.

* Corresponding author at: GPHI UMBC/NASA GSFC, Code 673, Greenbelt, MD 20771, USA.

E-mail addresses: Alexander.Lipatov-1@nasa.gov (A.S. Lipatov), David.G.Sibeck@nasa.gov (D.G. Sibeck).

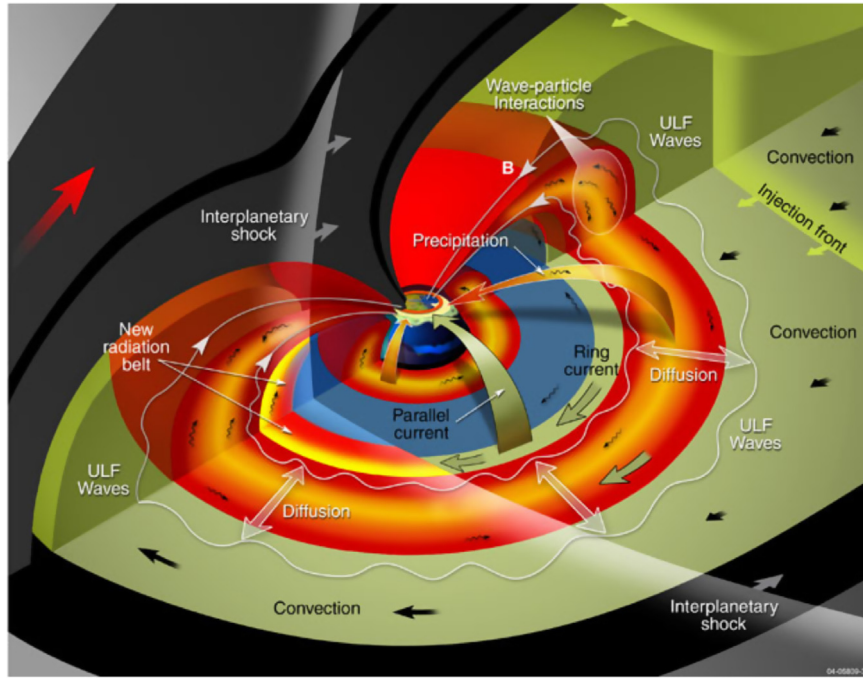


Fig. 1. Scheme of the Earth magnetosphere, radiation belts and propagation of the transmitted interplanetary shock (impulse) through the inner magnetosphere.

Since the particle distributions inside the transmitted interplanetary shock waves (impulses), ring current and radiation belts are essentially non-Maxwellian, wave-particle interactions play a very important role in the energy transport that occurs inside the inner magnetosphere. Finite ion gyroradius effects may also be important in mass loading the transmitted shock waves with the background plasma in the presence of higher energy ions and electrons from the ring current and radiation belts. To study these phenomena, we need a global hybrid code model. We use this model to study a shock front striking the magnetosphere.

During active conditions, the solar wind and the ionosphere provide rich sources of plasma to the geomagnetic tail (Chappell and Moore, 1987). Plasma sheet particles are transported earthward, energized, and trapped by the magnetic field of the Earth to form the ring current, whose electron component provides a seed population for the radiation belts (e.g., Jordanova, 2012). The anisotropic ring current ion and electron distributions generate diverse wave modes (electromagnetic ion cyclotron or EMIC, whistler, and magnetosonic), which may cause further particle acceleration and loss through energy and pitch angle scattering (e.g., Samsonov et al., 1998; Thorne and Horne, 1997; Thorne et al., 2006).

The majority of the plasma pressure in the Earth's inner magnetosphere is carried by ring current ions in the 1–200 keV energy range (Daglis et al., 1993). The westward drifting high-energy ions, and eastward drifting electrons, generate a ring current which intensifies significantly as geomagnetic activity increases (Le et al., 2004). The spatial and temporal development of the ring current considerably affects the magnetic field topology in the inner magnetosphere. There are several models for ring current dynamics, including the Ring current Atmosphere interactions Model with Self Consistent Magnetic field (see e.g. Dima et al., 2013; Jordanova et al., 2006). These models evaluate the bounce-averaged kinetic equation for the ion distribution function in the equatorial plane numerically. However, to study the interaction between shock waves and the ring current we need hybrid fluid-kinetic modeling, which will be the main method for our research.

The Earth has two radiation belts and sometimes more (e.g. a third belt ring of high-energy electrons) may be temporarily

created (Baker et al., 2013; Cole et al., 2013). The main belts cover altitudes from 1000 to 60,000 km above the surface. Energetic electrons form the outer belt, while protons and electrons form the inner belt. The belts endanger spacecraft, whose sensitive components must be adequately shielded if they spend significant time in the radiation belts.

This paper presents initial results from a new comprehensive multi-species global hybrid code that will be used to study the wave-particle interactions in the inner magnetosphere: transmitted shock (impulse) dynamics, deformation of the ring current, outer radiation belt and plasmasphere, dynamics of the ion velocity distribution function in the plasma structures. In Section 2 we formulate the problem and mathematical model. In Section 3 we describe the basic results from our modeling: the dynamics of the plasma structures, the transmitted shock dynamics and dynamics of the ion velocity distribution function in the ring current and outer radiation belt. The last section provides the conclusions of our research.

2. Computational model

We use a quasi-neutral hybrid model, namely, a kinetic description for the ions in the background plasma, the ring current, outer radiation belt and plasmasphere, and a fluid approximation for electrons to study the interaction between transmitted shocks and the inner magnetosphere. This model describes the wave-particle interactions on ion spatial and time scales ($\rho_{ci} = U_0/\Omega_i$ and $\omega \leq \Omega_i$) very well, where ρ_{ci} is the gyroradius for ions. U_0 and Ω_i denote the upstream velocity and the ion gyrofrequency. Our model takes into account ionization and charge exchange. The finite conductivity of the Earth's interior is also included. We will employ global hybrid code models to study the effects of various assumptions concerning shock orientation, strength, thickness, and magnetospheric particle distributions.

Fig. 1 presents an illustration of the interaction between the solar wind and the Earth magnetosphere. In our coordinate system, the X-axis is directed away from the Sun, the Y-axis is oriented in the direction of Earth's orbital motion and the Z-axis

completes the right-handed system. Note that the Earth is at $x = 0, y = 0, z = 0$. In our modeling we assume that there is no dipole tilt for the intrinsic magnetic field. It was only chosen to keep the simulation results simple and we can choose a more realistic initial magnetic field for interpretation of the observed data in future.

We assume that the mass and charge state of all ion populations under consideration are $M_s = M_p$ where M_p is a mass of protons, and $Z_s = 1$. In the current model we do not consider the inner radiation belt at $L < 2$, where L denotes the McIlwain shell parameter, which at the magnetic equator corresponds to the radial distance from the Earth's center expressed in units of Earth radii, R_E . In our modeling we choose $R_E = 6371$ km. In this paper we use a particle-mesh model for ion dynamics instead of the Vlasov/Boltzmann equation, Eq. (1).

Single ion particle motion is described by the equations:

$$\frac{d\mathbf{r}_{s,l}}{dt} = \mathbf{v}_{s,l} \quad (1)$$

and

$$\frac{d\mathbf{v}_{s,l}}{dt} = \frac{e}{M_s} \left(\mathbf{E} + \frac{\mathbf{v}_{s,l} \times \mathbf{B}}{c} \right). \quad (2)$$

The subscript s denotes the ion population ($s=1,2$ for background and plasmasphere ions, and $s=3,4$ for the H^+ outer radiation belt and ring current). The index l is the individual particle index in frame of particle-in-cell method.

In the nonradiative limit, Ampère's law is given by

$$\frac{4\pi}{c} \mathbf{J} = \nabla \times \mathbf{B}; \quad (3)$$

and the induction equation (Faraday's law) by

$$\frac{1}{c} \frac{\partial \mathbf{B}}{\partial t} + \nabla \times \mathbf{E} = 0. \quad (4)$$

The total current is given by

$$\mathbf{J} = \mathbf{J}_e + \mathbf{J}_i; \quad \mathbf{J}_i = \sum_{s=1}^{N_{\text{species}}} n_s \mathbf{U}_s = n_i \mathbf{U}_i, \quad (5)$$

where \mathbf{U}_s is the bulk velocity and n_i is the density of ions of type s ; n_i is the total ion density, and \mathbf{U}_i is the average ion bulk velocity.

The electron density is computed from the quasi-neutrality condition

$$n_e = n_{BG} + n_{RC} + n_{RB} + n_{PS} + n_{iono}. \quad (6)$$

Here, n_{BG} , n_{RC} , n_{RB} , n_{PS} , and n_{iono} denote the ion densities in the background plasma, ring current, outer radiation belt, plasmasphere and ionosphere.

For massless electrons the equation of motion of the electron fluid takes the form of the standard generalized Ohm's law (e.g. Braginskii, 1965):

$$\mathbf{E} = \frac{\mathbf{J}_e \times \mathbf{B}}{en_e c} - \frac{\nabla p_e}{en_e} \quad (7)$$

where $p_e = nm_e \langle v_e^2 \rangle / 3 = n_e T_e$ is the scalar electron pressure, and v_e is the thermal velocity of electrons; the electron current \mathbf{J}_e is estimated from Eq. (6).

For simplicity we assume that the total electron pressure may be represented as the sum of the partial pressures of all the electron populations:

$$p_e = p_{e0} \frac{(\beta_e n_{BG}^{5/3} + \beta_e n_{RC}^{5/3} + \beta_{e,RB} n_{RB}^{5/3} + \beta_{e,PS} n_{PS}^{5/3} + \beta_{e,iono} n_{iono}^{5/3})}{\beta_e n_0^{5/3}}, \quad (8)$$

where β_e , $\beta_{e,RC}$, $\beta_{e,RB}$, $\beta_{e,PS}$, and $\beta_{e,iono}$ denote the electron

background, plasmasphere, outer radiation belt and ionosphere betas. p_{e0} and n_0 are the shock (plasmasphere) electron pressure and ion density. We also assume here that $n_{e,BG} = n_{i,BG}$, $n_{e,RC} = n_{i,RC}$, $n_{e,RB} = n_{i,RB}$, $n_{e,PS} = n_{i,PS}$, and $n_{e,iono} = n_{i,iono}$. The same approach for the electron pressure was used in the modeling of the Europa's and Titan's plasma environment (see e.g. Lipatov et al., 2013a, 2014). Otherwise, we have to calculate the electron pressure from heat balance for electrons (see, e.g., Braginskii, 1965, Eq. (5) from Mankofsky et al., 1987) taking into account the electron heat fluxes, and the electron heating term. This equation works for highly collisional electrons ($\Omega_e \tau_e \ll 1$, where Ω_e and τ_e denote the electron cyclotron frequency and the characteristic electron collision time) but we believe that it is not the case for the electrons inside the ring current and outer radiation belt. The observations also show that electron populations in the ring current and radiation belt have a distinguish temperature. In this case equations for time evolution of the temperature for each species of electrons will be reduced into adiabatic process. In future modeling we also plan to estimate the electron pressure from the electron test particle tracing incorporated into our hybrid ion kinetic model.

In our model, the background plasma is homogeneous with a density of $5\text{--}10 \text{ cm}^{-3}$ (see e.g. Moldwin et al., 2002). Our background plasma does not include the plasmasphere. The plasmasphere is considered as a separate element. In our hybrid model we use a separate species for description of the ring current and outer radiation belt dynamics. Although the observations show that the ion temperatures are comparable in both population, the electron temperatures may be strongly distinct.

Ring current model: The ring current is one of the major current systems in the Earth's magnetosphere. It circles the Earth in the equatorial plane and is generated by the longitudinal drift of energetic ($10\text{--}200$ keV) charged particles trapped on field lines between $L \approx 2$ and 7 . During geomagnetic storms, ring current particle fluxes increase dramatically with peak enhancements occurring in the inner ring current (at $L < 4$). The quiet-time ring current consists predominantly of H^+ , while the storm-time ring current also contains a significant component of ionospheric O^+ , whose contribution to ring current energy density may even exceed that of H^+ for brief periods near the maximum of particularly intense storms. In our hybrid model the ring current may initially be a symmetrical or asymmetrical plasma solid torus. Our preliminary model is symmetric. Two parameters define the ring current structure: a major radius ($R_{RC} = 4.5R_E$) and a minor radius ($r_{RC} = 2.5R_E$), where R_{RC} is the distance from the center of the Earth to the center of the torus, and $2 \times r_{RC}$ is the width of the torus (see Fig. 2, top). Here, we use a homogeneous plasma density inside the current ring ($n \approx 3 \text{ cm}^{-3}$), however, the variable particle weights will allow us to produce an inhomogeneous density distribution in future models. The initial temperature of the ions in the ring current was chosen to be about $T_{i,RC} \approx 200$ keV in the preliminary modeling.

Outer radiation belt. In our model the outer radiation belt occupies the region between $L=3.5$ and $L=5.5$. In preliminary modeling we start from a homogeneous plasma density inside the outer radiation belt model ($n \approx 0.3 \text{ cm}^{-3}$), however, the variable particle weights will allow us to produce an inhomogeneous density distribution in future models (see Fig. 2, middle). The initial ion temperature was chosen to be about $T_{i,RB} \approx 200$ keV in preliminary modeling.

Plasmasphere. For the current symmetrical model for the plasmasphere we use an ion density profile consistent with the model suggested by Moldwin et al. (2002); Samsonov et al. (2011):

$$n_{PS} \propto n_{pp} 10^{(4.0 - 1.5 \cdot (r/R_E - 1) \cdot 3.5)} \quad (9)$$

Here, n_{PS} and n_{pp} denote the plasmasphere and plasmopause densities. In our preliminary modeling, the plasmopause is placed

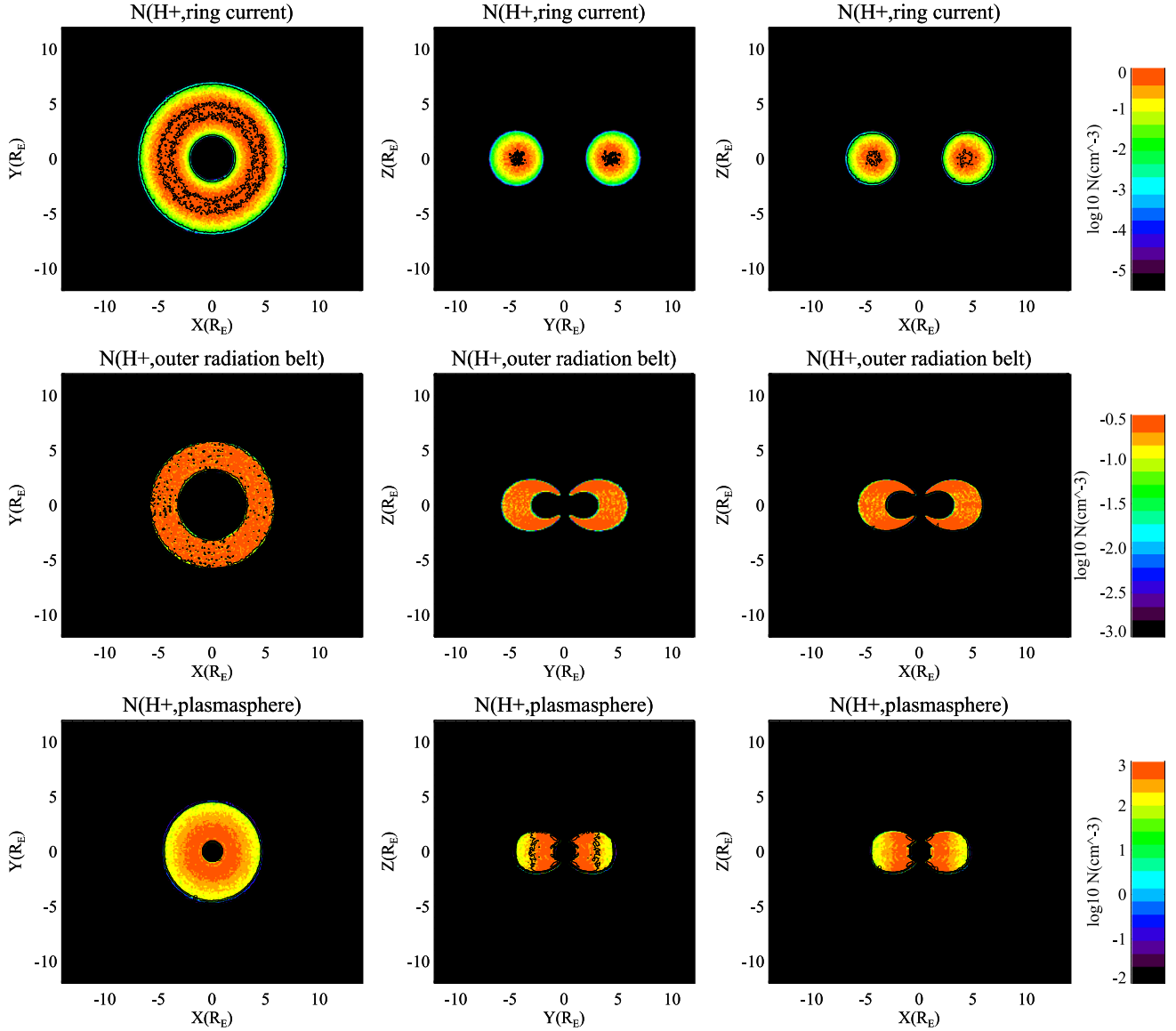


Fig. 2. Initial Conditions. 2-D cuts of the ring current, radiation belt and plasmasphere ion density profiles in the x - y , y - z and x - z planes. $t=0$.

at a distance $r = 4.5 R_E$ with a density of about $n_{pp} \approx 200 \text{ ion/cm}^3$. At $r = 2 R_E$ the plasma density is 1500 ion/cm^3 (see Fig. 2, bottom). The temperature of the ions was chosen to be about $T_{i,PS} \approx 1 \text{ eV}$. These parameters correspond to the model of Samsonov et al. (2011).

Ionosphere and Earth's interior. In the preliminary model, the ionosphere is approximated as an immobile plasma structure with small resistivity. The average ionospheric plasma density is about 10^3 cm^{-3} . In future modeling we will use a Hall-MHD approximation for the ionosphere to estimate the outflow flux due to ponderomotive forces. Such a model has already been used to study non-linear field line resonances (Lipatov and Rankin, 2005, 2009). The fluid and particle models will be coupled through the generalized Ohm's law (see e.g. Lipatov, 2002; Lipatov et al., 2002, 2005, 2012a, 2013b). The Earth is considered to be a solid body. The dipole geomagnetic field is fixed inside the Earth's interior.

At the flank boundaries, we apply a damping boundary condition for the electromagnetic field. At the downstream boundary a "Sommerfeld" radiation condition for the magnetic field and a free escape condition for particles has been applied. This boundary condition allows the re-entry of a portion of the particles from the outflow plasma. The upstream values of the magnetic field and

electric fields are $\mathbf{B} = \mathbf{B}_0$ and $\mathbf{E} = -\mathbf{U}_0 \times \mathbf{B}_0/c$.

We assume that ion bulk velocity is zero inside the Earth.

The particles are absorbed when they encounter the ionosphere surface. We do not use any boundary condition for the electromagnetic field at the Earth's surface. Inside the Earth, we use our equations for the electromagnetic field with internal conductivity and the ion bulk velocity. The variations of the value of the conductivity and ion bulk velocity across the ionosphere surface create a jump in the electric field.

We use a computational domain with the following dimensions $DX = 28 R_E$, $DY = 24 R_E$, and $DZ = 24 R_E$. The computational domain contains a grid of $561 \times 241 \times 241$ points, and 10^9 , 0.5×10^8 , 0.5×10^8 and 0.5×10^8 macro-particles for background, ring current, outer radiation belt and plasmasphere ions, respectively. To reduce the numerical shot noise we use variable mass macro-particles to generate the initial spatial distribution of ring current, radiation belt and plasmaspheric ions (see, e.g., Lipatov, 2012). In our modeling we use a 3-D rectangular box with the Earth's location shifted from the center of the computational domain depending on the problem to be simulated.

The numerical time step Δt_p for each particle push is chosen to satisfy the condition $\Delta t_p \leq \min(\Delta x, \Delta y, \Delta z)/(16_* v_{max})$, where v_{max}

denotes the maximum value of the macro-particle velocity. The numerical time step Δt_f for the electromagnetic field update is chosen to be $\Delta t_f \approx \Delta t_p/16$. The dimensional time steps are $\Delta t_p \approx 10^{-4}$ s and $\Delta t_f \approx 3 \times 10^{-6}$ s. This particle time step will provide good numerical approximation of the H^+ ion gyro rotation for a wide range of magnetic field ($\Omega_i \approx 1$ rad/s for $B \approx 10$ nT, $\Omega_i \approx 10^3$ rad/s for $B \approx 10^4$ nT). In the case of heavy ions, for example O^+ , a numerical approximation will be better.

The grid spacings are $\Delta_x \approx 335$ km, $\Delta_y \approx 670$ km and $\Delta_z \approx 670$ km. Note that the shock front normal is oriented quasi-parallel to the x -axis in the region close to the x -axis. The grid spacing in the x -direction will provide an approximation for spatial scales of several proton inertial lengths $c/\omega_{pi} = 228$ km ($n_{\text{background}} = 1 \text{ cm}^{-3}$) and $c/\omega_{pi} = 76$ km ($n_{\text{background}} = 10 \text{ cm}^{-3}$). Note that the coupling between the background plasma flow (impulse) and the ring current, and radiation belt ions excites low-frequency resonant and non-resonant waves (Winske et al., 1985) on these scales. The numerical approximation will be better in future modeling when it includes O^+ ions in the ring current and radiation belt.

The value of the ion gyroradii estimated for the shock front speed (≈ 1600 km/s) and the shock front speed plus the thermal velocity of upstream ions e.g. the ring current and outer radiation belt ions (≈ 3600 km/s) (see Section 3) are the following: (a) $\rho_{cp} \approx (1 - 3.6) \times 10^3$ km, $\rho_{co^+} \approx 5.5 \times 10^4$ km for $B = 10$ nT; (b) $\rho_{cp} \approx (1 - 3.6) \times 10^2$ km, $\rho_{co^+} \approx 5.5 \times 10^3$ km for $B = 100$ nT; (c) $\rho_{cp} \approx (1 - 3.6) \times 10$ km, $\rho_{co^+} \approx 5.5 \times 10^2$ km for $B = 1000$ nT. The mesh resolution will underestimate the ramp and foot of the shock wave in the proton background plasma at the initial stage for regions with $B = 10$ nT. At the latter time the shock wave becomes more dispersive. The spatial scale already exceeds the proton gyroradius due to the mass loading with the ring current and outer radiation belt protons. In future modeling the mesh will provide a good approximation of the gyroradius of the O^+ ions for regions with $B = 10$ nT and for $B = 100$ nT. In the region with $B = 1000$ nT the hybrid code will provide a drift-kinetic approximation for both proton and O^+ plasmas. In future modeling we plan to use adaptive mesh near the shock wave front to provide a good numerical resolution of the proton–electron subshock, ramp and foot inside the transmitted shock wave. 2.5-D hybrid models will also provide a fine numerical resolution to study the wave–particle interactions in the shock transition.

Initially the computational domain contains a homogeneous background plasma with a Maxwellian velocity distribution and plasma structures (the ring current, radiation belt and plasmasphere). The initial geomagnetic field was chosen to be a symmetrical dipole. At the left boundary, a step-like shock wave with finite thickness is introduced.

3. Modeling results

In our simulation of the interaction between transmitted shock (impulse) and the Earth's inner magnetosphere we have adopted the following sets of the solar wind and magnetosphere parameters in accordance with observations: upstream velocity, densities and magnetic field: $U_{\text{downstream}} \approx 1000$ km/s; initial thermal velocity $v_{\text{th,downstream}} = 200$ km/s and density in the region downstream from the shock $n_{\text{shock}} = 40 \text{ cm}^{-3}$; initial background plasma thermal velocity and density $v_{\text{th,BG}} = 20$ km/s and $n_{\text{BG}} = 10 \text{ cm}^{-3}$; the value of the magnetic field at the outer boundary ($x = -14 R_E$) $B_0 = 13.65$ nT. The energy of the protons and distances from the Earth to the center of the ring current (RC) are (0.01–1) MeV, $r_{\text{RC}} = 4.5 R_E$; outer radiation belt (RB), (0.1–10) MeV, $r_{\text{RB}} = 4.5 R_E$; and for the plasmasphere (PS) 1 eV, and

$r_{\text{PS}} = (1.1 - 4.4) R_E$. We choose the following electron energies in the ring current 30 keV, radiation belt (0.1–10) MeV and plasmasphere 50 eV.

3.1. Global interaction between the interplanetary transmitted shock and the inner magnetosphere

Studies of the interaction between transmitted shocks (impulses) and the inner Earth's magnetosphere need a self-consistent hybrid kinetic model for the nonstationary interaction of the solar wind with the geomagnetic field including the formation of the bow shock and magnetopause. These tasks include the interaction of the interplanetary shock with the bow shock and magnetopause, and the formation of the ring current, radiation belts and plasmasphere. The 1.5-D hybrid simulation of Cargill (1991) showed results from colliding shock interaction that strongly differ from those predicted by MHD simulations. We are still working on these tasks and we plan to present results from global modeling of nonstationary interaction with Earth's magnetosphere produced by MHD and hybrid codes in future.

MHD simulations of the interplanetary shock propagation through the inner magnetosphere (Samsonov et al., 2007, 2011, 2014; Kress et al., 2008; Halford et al., 2015) show that transmitted shock wave front has a step-like form. The thickness of the front is controlled by numerical diffusion. However, the dynamic of the shock wave transition will be important to understand the wave–particle interaction between the transmitted shock (impulse) and plasma structures inside the inner magnetosphere.

In the modeling presented here we use a simplified configuration of the inner magnetosphere and a step-like fast magnetosonic wave to represent the initial stage of the transmitted shock front inside the magnetopause. Such approach will be well enough to study the global effects of the above interaction. In future research we plan to use a multi-spacecraft observations (THEMIS) for input parameters of the transmitted shock waves. We expect that our hybrid model will support our data analysis and interpretation of the observations from THEMIS and Van Allen Probes mission.

In this modeling the bulk velocity downstream from the shock is about 1000 km/s, while the density jump is about 4, so the speed of the shock front is about $U_{\text{shock}} \approx 1600$ km/s. Note that we have performed preliminary modeling for a wide range of bulk velocities downstream from the shock and density jumps.

Despite these simplifications, the model suffices to study the deformation of the ring current, outer radiation belt, and plasmasphere by the transmitted shock.

The initial configuration of the inner magnetosphere's elements includes axi-symmetric distributions for the ring current, outer radiation belt and plasmasphere. These distributions are shown in Fig. 2. The initial distribution of the background plasma and the perturbation in the magnetic field are shown in Fig. 3. One can see the initial transmitted shock configuration in Fig. 3 (top and bottom). Figs. 2 and 3 show the planer shock entering the simulation domain from the sunward ($-X$) side.

While the transmitted impulse propagates through the inner magnetosphere, the shock front interacts with particles in the ring current and outer radiation belt first and then plasmaspheric particles. A portion of the transmitted impulse passes freely through the outer part of the inner magnetosphere. Figs. 4, 5 and 6 present 2-D cuts of the plasma density profile for the ring current, outer radiation belt, plasmasphere, background plasma and variations in the magnetic field ($B - B_{\text{dipole}}$) produced in the 3-D global hybrid model at time $t \approx 120$ s. One can see a strong deformation of the ring current, outer radiation belt, and plasmasphere density profiles while they interact with the transmitted interplanetary shock front. Such strong spatial perturbations play a

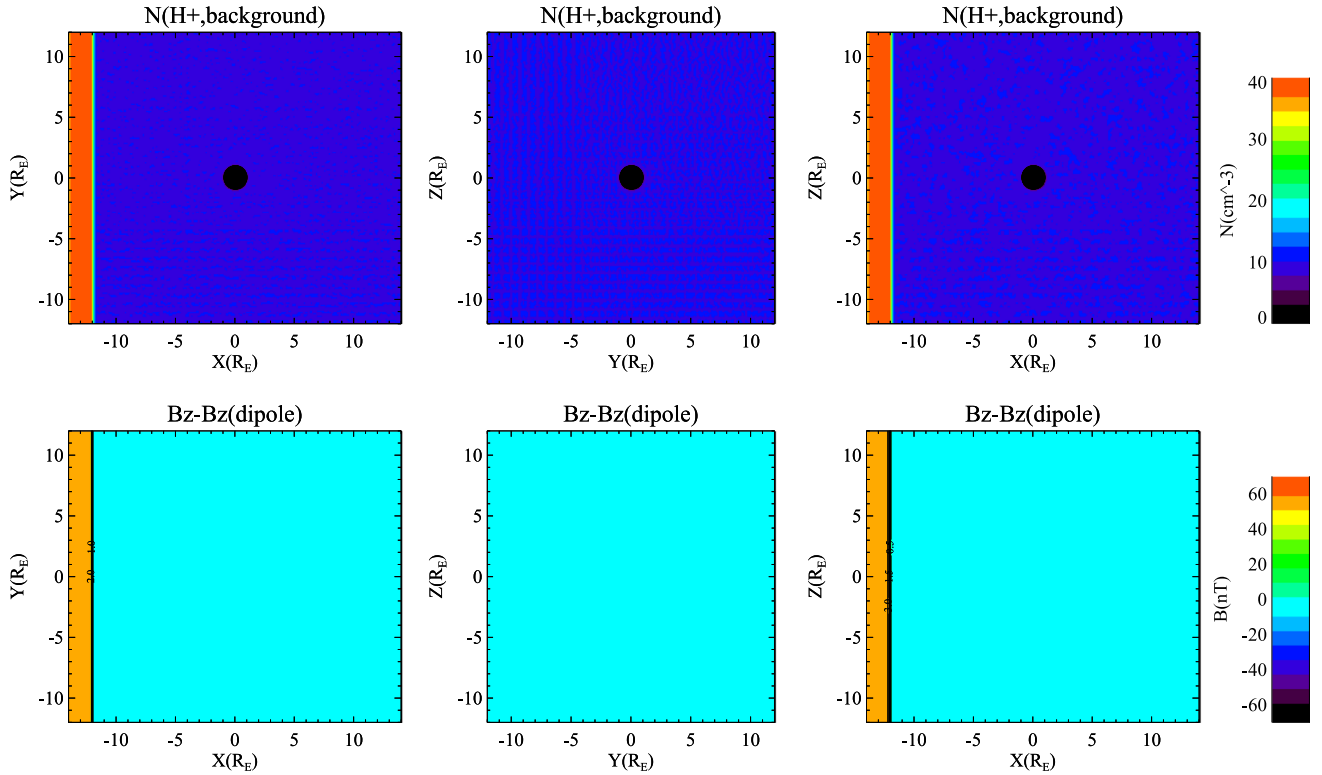


Fig. 3. Initial Conditions. 2-D cuts of background ion density and magnetic field profiles in x - y and y - z and x - z planes. The transmitted shock has a step-function profile and it was setup at the left boundary (red-density, green-magnetic field), $t=0$. (For interpretation of the references to color in this figure caption, the reader is referred to the web version of this paper.)

key role in the particle acceleration/deceleration. These strong spatial perturbations may be related to the Richmyer–Meshkov and Rayleigh–Taylor instabilities which were observed in stellar explosions (e.g. Drake et al., 2009). The perturbations in the plasma density profiles have a spatial scale from $1 R_E$ to a few R_E . It seems that these perturbations are not related to the “shot” noise effects. However, we need further investigation of these instabilities. The center panels of Fig. 4 with z - y density profiles clearly show a rather substantial dawn–dusk asymmetry for all populations. We guess that those asymmetric distributions are results of the finite ion gyroradius effects. The right-hand panels of Fig. 4 with x - z density profiles show plasma compression in the day side and an expansion at the night side. The large scale perturbations were observed by Van Allen Probes measurements presented in Gallton et al. (2015), Keika et al. (2015), and Kempf et al. (2015). The authors explain the generation of these perturbations in term of heavy ring current ions interacting with ULF waves.

The transmitted shocks in the equatorial plane have a quasi-perpendicular structure whereas those transmitted near the cusp region have a quasi-parallel structures.

In the higher latitude regions near “the cusps”, the transmitted shock wave has a quasi-parallel structure and propagates much faster and deeper into the plasmasphere than near the equatorial plane. The parallel plasma beam driven by transmitted shock near the “cusp” is compressed by convergence of the magnetic field while the particles move toward the ionosphere. This plasma beam can disturb the plasmasphere and the inner radiation belt through the wave–particle interaction. To study wave–particle interactions at the front of the interplanetary collisionless shock wave we would need to perform 2.5-D and 1.5-D hybrid kinetic modeling with fine resolution at the shock front. Our future modeling will provide an opportunity to study particle heating and acceleration at the front of a collisionless shock in the ring

current and radiation belts, structuring and instabilities in the shock transition.

The transmitted shock (impulse) compresses magnetic field lines in the equatorial plane and deforms magnetic field lines in the meridional plane. Fig. 5 (bottom) shows perturbations generated in the magnetic field component ($B_z - B_{z,dipole}$). One can see a strong compression at dawn and dusk region (middle column) with a maximum at the equatorial plane. Such a compression will generate an Alfvén waves propagating along the magnetic field lines in agreement with 3-D modeling using the Dungey equations (Lipatov, 1972; Van’yan and Lipatov, 1974a,b).

Near the equatorial plane one can also see small-scale perturbations in the magnetic field component ($B_z - B_{z,dipole}$) in the dayside ($5 < L < 8$) and nightside regions ($3 < L < 8$). Small amplitude and scale perturbations in the magnetic field components ($B_x - B_{x,dipole}$) and ($B_y - B_{y,dipole}$) were also observed in the same region as for ($B_z - B_{z,dipole}$), Fig. 6 (top and bottom, left and column columns). We suppose that these perturbations may be related to the electromagnetic ion cyclotron waves.

3.2. Thin structure of the transmitted shock (impulse) in the inner magnetosphere

Our next step will be to analyze the wave–particle interactions upstream and downstream of the transmitted shock. The structure of the collisionless shock wave front is a key factor for understanding particle heating and acceleration inside the ring current and radiation belts.

Inside the inner magnetosphere the transmitted shock wave fronts are mass loaded with energetic particles from the ring current and radiation belts. These higher energy particles may be treated as pickup ions in the rest frame of the shock. A portion of the kinetic energy of the plasma flow goes over into cyclotron gyration energy of the pickup ions. The irreversibility of such a

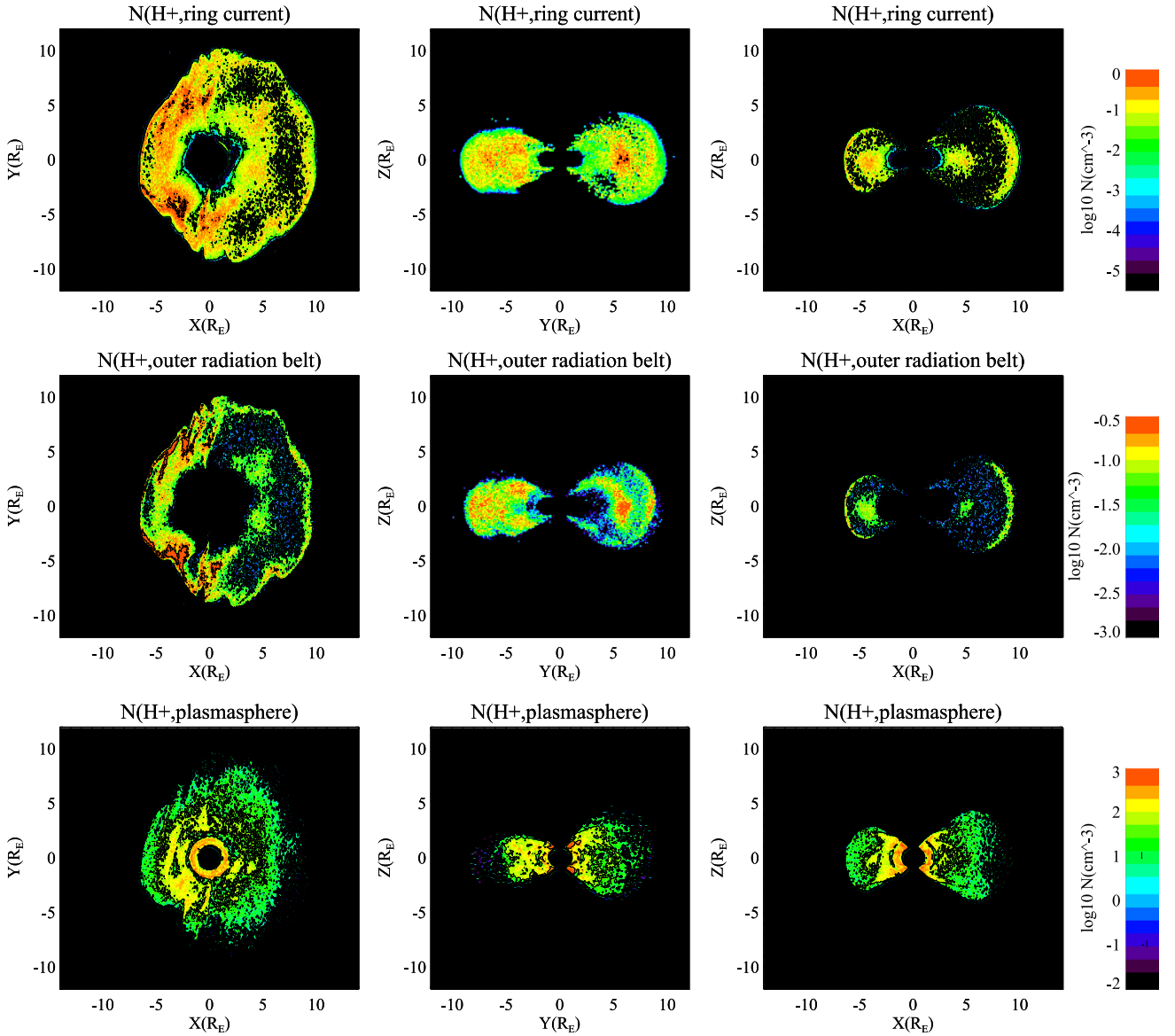


Fig. 4. After the passage of the shock. 2-D cuts of the ring current, radiation belt and plasmasphere ion density profiles in the x-y, y-z and x-z planes. Transmitted shock deforms and may even destroy the ring current, radiation belt, and plasmasphere. $t \approx 70$ s.

transition (e.g. shock waves) is associated with the mixing of the phases of the cyclotron gyration of the ions in the strongly inhomogeneous magnetic field at the wave front (Galeev et al., 1985).

Fig. 7 shows the time evolution of the shock front during the shock wave propagation through the inner magnetosphere. One can see the formation of perturbations as a result of the interaction of the shock front with the ring current, radiation belt and plasmapause. At an early stage ($t < 9.4$ s), there is no mass loading of the transmitted shock with the ring current ions and the shock front takes the form of an overshoot with a density jump of 6 preceded by a foot/precursor with a density jump of about 2. By $t \approx 17$ s, the overshoot profile has changed and the foot is already perturbed by mass loading with the ring current ions. By $t \approx 22.5$ s, the shock structure has changed a lot by mass loading with ions from the ring current and outer radiation belt. A portion of the background plasma flux reflected by encounters with the ring current and outer radiation belt produces a strong jump in the density profile that moves sunward in the direction of the magnetopause (red arrow). In this regime the plasma dynamics inside the transmitted and reflected shock wave is considered to be an

inter-penetrating flow. At a time $t > 22.5$ s, the reflected shock continues to move sunward in the direction of the magnetopause with generation of the mirror-type instability downstream of the shock front. The jump in the overshoot density profile is more than 2.5. The over-all background density profile becomes irregular due to the excitation of low-frequency waves triggered by non-Maxwellian ion velocity distributions and the wavelength of these oscillations are in the range from 1000 km to 2000 km, Fig. 7 (bottom).

Depending on the shock structure and energy distribution of the pickup ions (ring current and radiation belt particles), the particles can be accelerated to some fixed value of the energy by shock surfing (multiple reflections) at the shock front (see Lipatov and Zank, 1999; Lipatov, 2002, 2012). Further acceleration may be produced by the electromagnetic waves excited near the shock front (Lipatov et al., 1998). Fig. 8 shows examples of background and ring current ion velocity distribution just downstream from the shock front. One can see anisotropic background and ring current ion velocity distributions with $T_{BG,\perp}/T_{BG,\parallel} \approx 9$ and $T_{RC,\perp}/T_{RC,\parallel} \approx 5$. Such anisotropic ion velocity distributions can

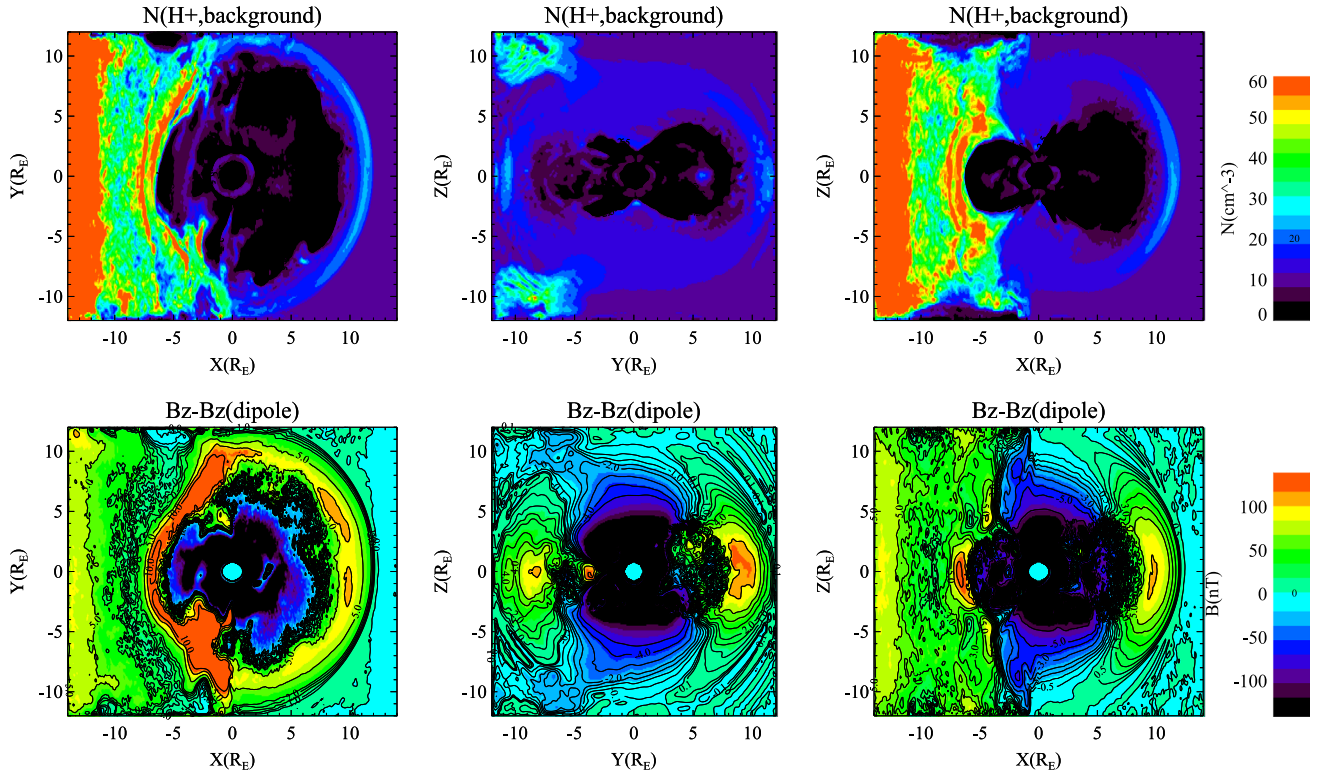


Fig. 5. After the passage of the shock. 2-D cuts of background ion density and magnetic field ($B_z - B_{z,dipole}$) profiles in x - y and y - z and x - z planes. Mass loading of ring current and radiation belt plays an important role in shock formation and structure. The shock front asymmetry shown in the top in the middle is due to the finite ion gyroradius and “shot” noise effects. In the higher latitude near the cusps regions, the shock front propagates much faster and deeper toward the ionosphere. Shock front has a quasi-parallel structure and it may create the ion beam along the geomagnetic field. 3-D perturbations in magnetic field have a complicated structure. $t \approx 70$ s.

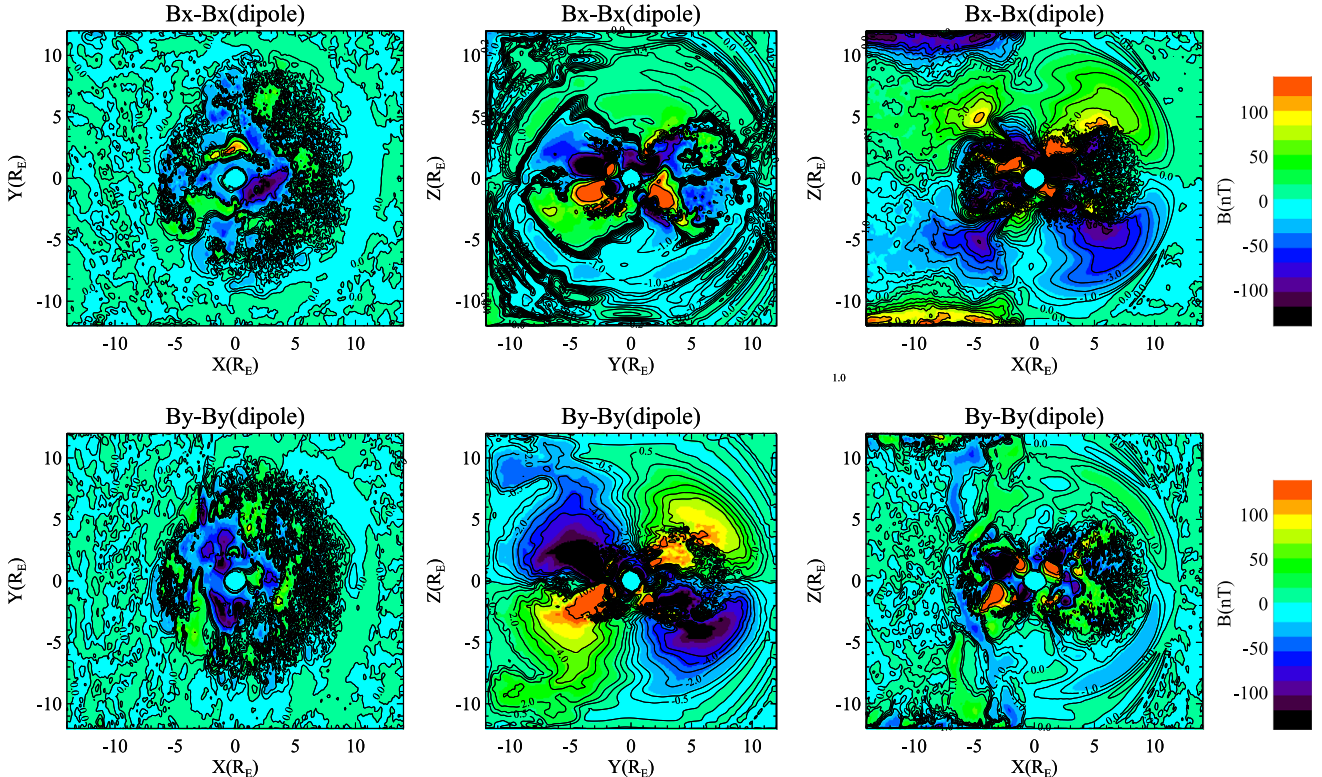


Fig. 6. After the passage of the shock. 2-D cuts of the perturbations in the magnetic field ($B_x - B_{x,dipole}$), ($B_y - B_{y,dipole}$) profiles in x - y and y - z and x - z planes. 3-D perturbations in magnetic field have a complicated structure. $t \approx 70$ s.

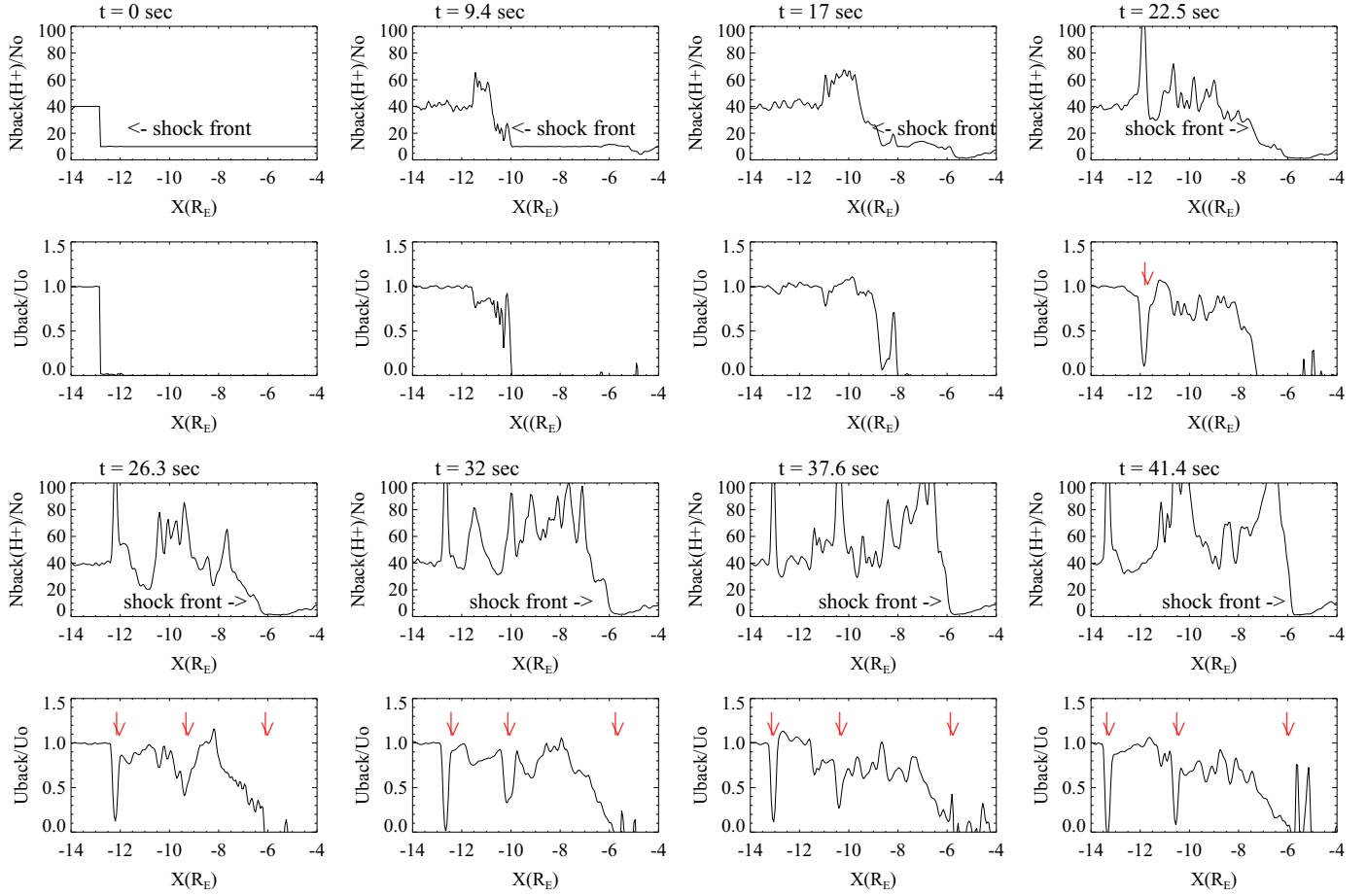


Fig. 7. Shock time dependent structure. One can see a partial reflection of shock by ring current, radiation belt and plasmopause (red arrows). Arrows point to low flow velocities where a reflected shock has slowed the oncoming magnetosheath flow. $U_{\text{downstream}} = 1000$ km/s. (For interpretation of the references to color in this figure caption, the reader is referred to the web version of this paper.)

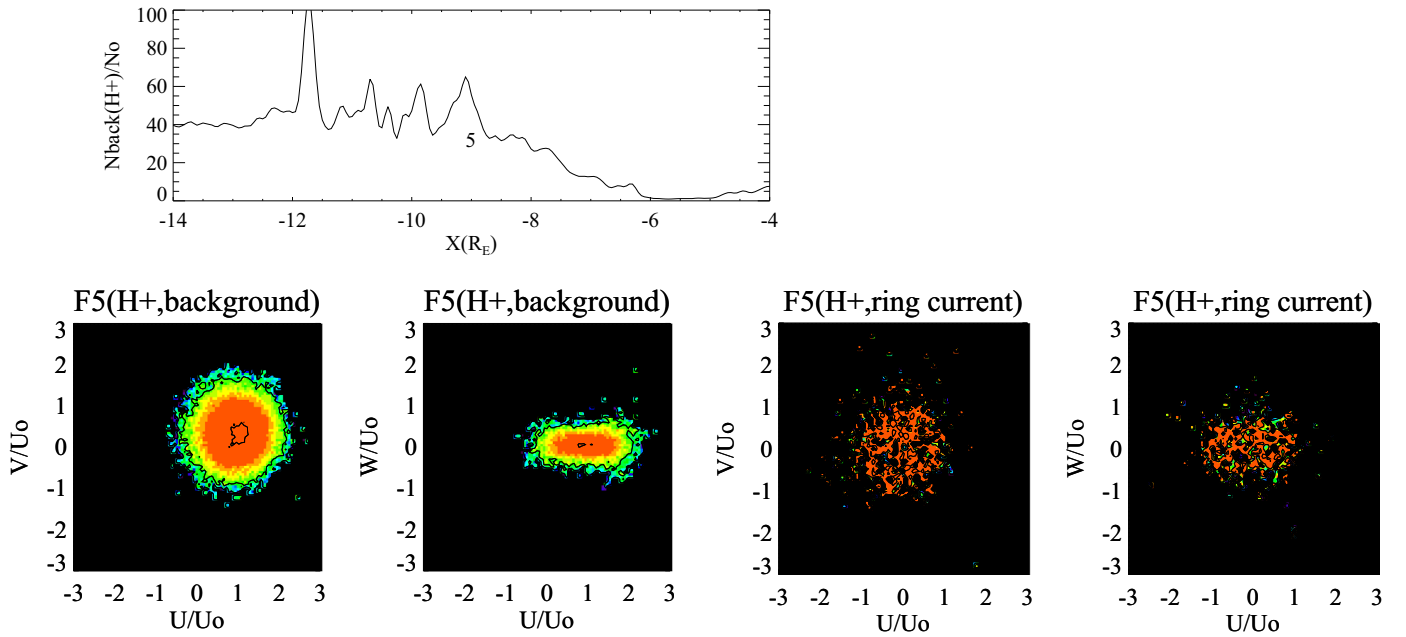


Fig. 8. Example of non-Maxwellian ion velocity distribution functions (VDFs) for the background and ring current plasma at the location N.5 (bottom). $t \approx 40$ s. The spatial location of the VDFs shown with the number 5 in the 1-D cut of the background plasma density profile (top). The passage of the shock generates non-Maxwellian velocity distribution functions that can trigger waves and instabilities. This figure shows anisotropic ion velocity distributions downstream from the shock front. The velocities V and U are perpendicular to the geomagnetic field whereas the velocity W is parallel to the geomagnetic field.

trigger the ballooning-mirror instability (Cheng and Qian, 1994; Cheng et al., 1994; Korotova et al., 2013) and excite non-linear magnetic field line resonances (Lipatov and Rankin, 2005, 2009). THEMIS-A observations confirmed the formation of the anisotropic distribution of energetic ring current ions (see Fig. 4, bottom from Zhang et al., 2012), with energies of a few tens keV. The authors expect that such anisotropic ion velocity distribution will excite EMIC waves. A more detailed analysis of the ion velocity distribution dynamics will be presented in a future publication.

4. Conclusions

Initial results from a hybrid kinetic model for Earth's plasma environment with four (background, ring current, radiation belt and plasmaspheric) ion species has demonstrated several features:

1. Mass loading of the transmitted shock (impulse) by ring current and radiation belt ions results in strong variations in the shock foot, overshoot and downstream plasmas. The shock exhibits time-dependent structure as it propagates through the magnetosphere.
2. The passage of the shock generates non-Maxwellian velocity distribution functions with an anisotropy from 5 to 9 that can trigger waves and instabilities like a mirror-ballooning instability.
3. Transmitted shocks deform the ring current, radiation belt and plasmasphere.
4. The transmitted shock (impulse) compresses magnetic field lines in the equatorial plane and deforms magnetic field lines in the meridional plane.
5. A strong compression in the dawn-dusk region (middle column) with a maximum in the equatorial plane will result in the generation of Alfvén waves propagating along the magnetic field lines.
6. Near the equatorial plane one can also see small-scale perturbations in the magnetic field components ($B_z - B_{z,dipole}$), ($B_x - B_{x,dipole}$) and ($B_y - B_{y,dipole}$) located in the dayside ($5 < L < 8$) and nightside regions ($3 < L < 8$). We suppose that these perturbations may be related to the electromagnetic ion cyclotron waves.
7. In the higher latitude region near “the cusp”, the transmitted shock wave has a quasi-parallel structure and it propagates much faster and deeper into the plasmasphere than near the equatorial plane. The parallel plasma beam near the “cusp” will be compressed by convergence of the magnetic field while the particles approach the ionosphere.

The study of the interaction between shock waves (impulses) and the radiation belt has a broad impact on understanding the plasma processes inside the inner magnetospheres of planets, possible plasma processes in the solar flares, and the plasma processes that govern the generation of the “third” radiation belt.

In future work we expect to compare our predictions with observations from the THEMIS and Van Allen Probes spacecraft on October 8, 2013 from Foster et al. (2015). Current spacecraft configurations offer unique opportunities to study the magnetospheric response to interplanetary shocks. These data will provide information about the wave-particle interactions, in particular the heating and acceleration of the particles in the ring current and radiation belts. We also expect to include a magnetotail in our model to study the interaction between transmitted impulses and the plasma sheet. Several previous 2.5-D ion kinetic modeling (see e.g. Lipatov and Zelenyi, 1979) have already shown the importance wave-particle interactions, non-Maxwellian velocity distributions in the particle heating and acceleration in the plasma sheet.

Acknowledgments

This work was supported in part by the NASA mission “Van Allen Storm Probes”. Computational resources were provided for the High-End Computational Project SMD-15-5719, “Shock waves interaction with plasmasphere and radiation belts. hybrid fluid-kinetic modeling” by the NCCS (Discover, Goddard) and the NAS (Pleiades, Ames).

References

- Baker, D.N., Kanekal, S.G., Hoxle, V.C., Henderson, M.G., Li, X., Spence, H.E., Elkington, S.R., Fridel, R.H.W., Goldstein, J., Hudson, M.K., Reeves, G.D., Thome, R. M., Kletzing, C.A., Claudepierre, 2013. A long-lived relativistic electron storage ring embedded in Earth's outer Van Allen belt. *Science* 340, 186–190, <http://dx.doi.org/10.1126/science.1233518>.
- Braginskii, S.L., 1965. Transport processes in a plasma. In: Leontovich, M.A. (Ed.), *Reviews of Plasma Physics*. Consultants Bureau, New York, pp. 205–240.
- Cargill, P.J., 1991. The interaction of collisionless shocks in astrophysical plasmas. *Astrophys. J.* 376, 771–781.
- Chappell, C.R., Moore, T.E., Waite Jr., J.H., 1987. The ionosphere as a fully adequate source of plasma for the Earth's magnetosphere. *J. Geophys. Res.* 92 (A6), 5896–5910.
- Cheng, C.Z., Qian, Q., 1994. Theory of ballooning-mirror instabilities for anisotropic pressure plasmas in the magnetosphere. *J. Geophys. Res.* 99 (A6), 11193–11209.
- Cheng, C.Z., Qian, Q., Takahashi, K., Lui, A.T.Y., 1994. Ballooning-mirror instability and internally driven Pc 4–5 wave events. *J. Geomagn. Geoelectr.* 46, 997–1009.
- Cole, S., Snider, L.C., Brown, G., 2013. NASA's Van Allen probes reveal a new radiation belt around Earth. *ScienceDaily*, February 28, 2013, Release 13-065.
- Daglis, I.A., Sarris, E.T., Wilken, B., 1993. AMPTE/CCE CHEM observations of the energetic ion population at geosynchronous altitudes. *Ann. Geophys.* 11, 685–696.
- Dima, G., Jordanova, V., Yu, Y., 2013. Modeling ring current dynamics using the RAM-SCB inner magnetosphere model. In: Los Alamos SpaceWeather Summer School, Report 2013, pp. 1–10.
- Drake, R.P., Kuranz, C.C., Miles, A.R., Muthsam, H.J., Plewa, T., 2009. Stellar explosions, instabilities, and turbulence. *Phys. Plasmas* 16, 041004.
- Elkington, S.R., Hudson, M.K., Witberger, M.J., Lyon, J.G., 2002. MHD/particle simulations of radiation belt dynamics. *J. Atmos. Sol.-Terr. Phys.* 64, 607–615.
- Fujita, S., Tanaka, T., Kikuchi, T., Fujimoto, K., Hosokawa, K., Itonaga, M., 2003a. A numerical simulation of the geomagnetic sudden commencement: 1. Generation of the field-aligned current associated with the preliminary impulse. *J. Geophys. Res.* 108 (A12), 1416. <http://dx.doi.org/10.1029/2002JA009407>.
- Fujita, S., Tanaka, T., Kikuchi, T., Fujimoto, K., Itonaga, M., 2003b. A numerical simulation of the geomagnetic sudden commencement: 2. Plasma processes in the main impulse. *J. Geophys. Res.* 108 (A12), 1417. <http://dx.doi.org/10.1029/2002JA009763>.
- Fujita, S., Tanaka, T., Motoba, T., 2005. A numerical simulation of the geomagnetic sudden commencement: 3. A sudden commencement in the magnetosphere-ionosphere compound system. *J. Geophys. Res.* 110 (A11), 203. <http://dx.doi.org/10.1029/2005JA011055>.
- Foster, J.C., Wygant, J.R., Hudson, M.K., Boyd, A.J., Baker, D.N., Erickson, P.J., Spence, H.E., 2015. Shock-induced prompt relativistic electron acceleration in the inner magnetosphere. *J. Geophys. Res.* 120 (3), 1661–1674.
- Galeev, A.A., Lipatov, A.S., Sagdeev, R.Z., 1985. Numerical simulation of shock waves near comets: structural features and energy dissipation mechanisms. *Sov. Phys. JETP* 62 (5), 866.
- Gallton, A., et al., 2015. Overview of radiation belt storm probes ion composition experiment (RBSPICE): data access and science results. Fall AGU Meeting, December 14–18, 2015, San Francisco, CA, ID: SM41E-2517.
- Glocer, A., Toth, G., Ma, Y., Gombosi, T., Zhang, J.-C., Kistler, L.M., 2009. Multifluid block-adaptive-tree solar wind roe-type upwind scheme: magnetospheric composition and dynamics during geomagnetic storms—initial results. *J. Geophys. Res.* 114, A12203. <http://dx.doi.org/10.1029/2009JA014418>.
- Gutynska, O., Sibeck, D.G., Omid, N., 2015. Magnetosheath plasma structures and their relation to foreshock processes. *J. Geophys. Res. Space Phys.* 120, 7687–7697. <http://dx.doi.org/10.1002/2014JA020880>.
- Halford, A.J., McGregor, S.L., Murphy, K.R., Millan, R.M., Hudson, M.K., Woodger, L.A., Cattel, C.A., Breneman, A.W., Mann, I.R., Kurth, W.S., Hospodarsky, G.B., Gkioulidou, M., Fennel, J.F., 2015. BARREL observations of an ICME-shock impact with the magnetosphere and the resultant radiation belt electron loss. *J. Geophys. Res. Space Phys.* 120, 2557–2570. <http://dx.doi.org/10.1002/2014JA020873>.
- Hudson, M.K., Kotelnikov, A.D., Li, X., Roth, I., Temerin, M., Wygant, J., Blake, J.B., Gussenhoven, M.S., 1995. Simulation of proton radiation belt formation during the March 24, 1991 SSC. *Geophys. Res. Lett.* 22 (3), 291–294 1995.
- Hudson, M.K., Kress, B.T., Mueller, H.R., Zastrow, J.A., Blake, J.B., 2008. Relationship of the Van Allen radiation belts to solar wind driver. *J. Atmos. Solar-Terr. Phys.* 70, 708–729.
- Hudson, M.K., Paral, J., Kress, B.T., Wiltberger, M., Baker, D.N., Foster, J.C., Turner, D. L., Wygant, J.R., 2015. Modeling CME-shock-driven storms in 2012–2013: MHD

- test particle simulations. *J. Geophys. Res. Space Phys.* 120, 1168–1181. <http://dx.doi.org/10.1002/2014JA020833>.
- Jordanova, V.K., 2012. The role of the Earth's ring current in radiation belt dynamics. In: Summers, D., Mann, I.R., Baker, D.N., Schulz, M. (Eds.), *Dynamics of the Earth's radiation belts and inner magnetosphere*, vol. 199. AGU Monographs, Washington, DC, <http://dx.doi.org/10.1029/2012GM001330>.
- Jordanova, V.K., Miyoshi, Y.S., Zaharia, S., Thomsen, M.F., Reeves, G.D., Evans, D.S., Mouikis, C.G., Fennell, J.F., 2006. Kinetic simulations of ring current evolution during the geospace environment modeling challenge events. *J. Geophys. Res.* 111, A11S10. <http://dx.doi.org/10.1029/2006JA011644>.
- Keika, K., Seki, K., Nose, M., et al., 2015. Characteristics of ring current protons and oxygen ions during the 7 January 2015 and 17 March 2015 storms: Van Allen Probes/RBSPICE observations. Fall AGU Meeting, December 14–18, 2015, San Francisco, CA, ID: SM41E-2534.
- Kempf, Y., Pokhotelov, D., Gutynska, O., Wilson III, L.B., Walsh, B.M., von Althaus, S., Hunnuksela, O., Sibeck, D.G., Palmroth, M., 2015. Ion distributions in the Earth's foreshock: hybrid-Vlasov simulation and THEMIS observations. *J. Geophys. Res. Space Phys.* 120, 3684–3701. <http://dx.doi.org/10.1002/2014JA020519>.
- Kim, H., Lanzerotti, L.J., Gerrard, A.J., et al., 2015. Study of interactions between ULF waves and ring current heavy (He⁺ and O⁺) ions. Fall AGU Meeting, December 14–18, 2015, San Francisco, CA, ID: SM41F-2553.
- Korotova, G.I., Sibeck, D.G., Angelopoulos, V., Walsh, B.M., 2013. THEMIS observations of compressional poloidal pulsations in the dawnside magnetosphere: a case study. *J. Geophys. Res.* 118, 7665–7673. <http://dx.doi.org/10.1002/2013JA019360>.
- Kress, B.T., Hudson, M.K., Looper, M.D., Lyon, J.G., Goodrich, C.C., 2008. Global MHD test particle simulations of solar energetic electron trapping in the Earth's radiation belts. *J. Atmos. Sol.-Terr. Phys.* 70, 1727–1737.
- Le, G., Russell, C.T., Takahashi, K., 2004. Morphology of the ring current derived from magnetic field observations. *Ann. Geophys.* 22, 1267–1295.
- Lin, Y., Wang, X.Y., 2005. Three-dimensional global hybrid simulation of dayside dynamics associated with the quasi-parallel bow shock. *J. Geophys. Res.* 110, A12216. <http://dx.doi.org/10.1029/2005JA011243>.
- Lipatov, A.S., 1972. The propagation of hydromagnetic waves in the three-dimensional model of the magnetosphere, Candidate of Sciences (Ph.D. dissertation). Moscow Institute of Physics and Technology (State Univ.), Moscow.
- Lipatov, A.S., 2002. The Hybrid Multiscale Simulation Technology: An Introduction With Application to Astrophysical and Laboratory Plasmas. Monograph, Springer-Verlag, Berlin, Heidelberg, New York, pp. 403.
- Lipatov, A.S., 2012. Merging for particle-mesh complex particle kinetic modeling of the multiple plasma beams. *J. Comput. Phys.* 231, 3101–3118.
- Lipatov, A.S., Cooper, J.F., Sittler, E.C., Hartle, R.E., 2012a. Effects of Na⁺ and He⁺ pickup ions on the lunar-like plasma environment: 3-D hybrid modeling. *Adv. Space Res.* 50, 1583–1591.
- Lipatov, A.S., Cooper, J.F., Paterson, W.R., Sittler Jr., E.C., Hartle, R.E., Simpson, D.G., 2013a. Jovian plasma torus interaction with Europa. Plasma wake structure and effect of inductive magnetic field: 3D hybrid kinetic simulation. *Planet. Space Sci.* 77, 12–24. <http://dx.doi.org/10.1016/j.pss.2013.01.009> (Part VIII March 2013).
- Lipatov, A.S., Cooper, J.F., Sittler Jr., E.C., Hartle, R.E., 2013b. The light (H⁺, H₂⁺, He⁺) and heavy (Na⁺) pickup ion dynamics in the lunar-like plasma environment: 3D hybrid kinetic modeling. *Adv. Space Res.* 52, 1929–1938.
- Lipatov, A.S., Motschmann, U., Bagdonat, T., 2002. 3D hybrid simulations of the interaction of the solar wind with a weak comet. *Planet. Space Sci.* 50, 403–411.
- Lipatov, A.S., Motschmann, U., Bagdonat, T., Griessmeier, J.-M., 2005. The interaction of the stellar wind with an extrasolar planet – 3-D hybrid and drift-kinetic simulations. *Planet. Space Sci.* 53, 423–432.
- Lipatov, A.S., Rankin, R., 2005. Multi-Fluid and kinetic modeling of nonlinear field line resonances. Meeting of the Department of Aeronomy and Space Physics (DASP) of the Canadian Association of Physics, February 22–26, 2005, Crowne Plaza Chateau Lacombe, Edmonton and Athabasca University, Athabasca.
- Lipatov, A.S., Rankin, R., 2009. Nonlinear field line resonances. Effect of Hall term on plasma compression: 1D Hall-MHD modeling. *Planet. Space Sci.* 57, 404–414.
- Lipatov, A.S., Sittler Jr., E.C., Hartle, R.E., Cooper, J.F., Simpson, D.G., 2014. Titan's plasma environment: 3D hybrid kinetic modeling of the TA flyby and comparison with CAPS-ELS and RPWS LP observations. *Planet. Space Sci.* 93–94 (April), 119–128. <http://dx.doi.org/10.1016/j.pss.2014.02.012>.
- Lipatov, A.S., Zank, G.P., 1999. Pickup ion acceleration at low- β_p perpendicular shocks. *Phys. Rev. Lett.* 82 (18), 3609.
- Lipatov, A.S., Zank, G.P., Pauls, H.L., 1998. The acceleration of pickup ions at shock waves: test particle-mesh simulations. *J. Geophys. Res.* 103 (A12), 29679–29696.
- Lipatov, A.S., Zelenyi, L.M., 1979. Dynamics of magnetic field reconnection in a neutral sheet as an Alfvén pulse passes. *Sov. J. Plasma Phys.* 5 (4), 525.
- Mankofsky, A., Sudan, R.N., Denavit, J., 1987. Hybrid simulation of ion beams in background plasma. *J. Comput. Phys.* 70, 89–116.
- Moldwin, M.B., Downward, L., Rassoul, H.K., Amin, R., Anderson, R.R., Downward, L., 2002. A new model of the location of the plasmapause: CRRES results. *J. Geophys. Res.* 107 (A11), 1339. <http://dx.doi.org/10.1029/2001JA009211>.
- Omid, N., Zhang, H., Sibeck, D., Turner, D., 2013. Spontaneous hot flow anomalies at quasi-parallel shocks: 2. Hybrid simulations. *J. Geophys. Res.* 118, 173–180. <http://dx.doi.org/10.1029/2012JA018099>.
- Omid, N., Sibeck, D., Gutynska, O., Trattner, K.J., 2014. Magnetosheath filamentary structures formed by ion acceleration at the quasi-parallel bow shock. *J. Geophys. Res. Space Phys.* 119, 2593–2604. <http://dx.doi.org/10.1002/2013JA019587>.
- Samsonov, A.A., Sibeck, D.G., Imber, J., 2007. MHD simulation for the interaction of an interplanetary shock with the Earth's magnetosphere. *J. Geophys. Res.* 112, A12220. <http://dx.doi.org/10.1029/2007JA012627>.
- Samsonov, A.A., Sibeck, D.G., Walsh, B.M., Zolotova, N.V., 2014. Sudden impulse observations in the dayside magnetosphere by THEMIS. *J. Geophys. Res.* 119, 9476–9496. <http://dx.doi.org/10.1002/2014JA020012>.
- Samsonov, A.A., Sibeck, D.G., Zolotova, N.V., Biernat, H.K., Chen, S.-H., Rastaetter, L., Singer, H.J., Baumjohann, W., 2011. Propagation of a sudden impulse through the magnetosphere initiating magnetospheric Pc5 pulsations. *J. Geophys. Res.* 116, A10216. <http://dx.doi.org/10.1029/2011JA016706>.
- Summers, D., Thorne, R.M., F. Xiao, F., 1998. Relativistic theory of wave-particle resonant diffusion with application to electron acceleration in the magnetosphere. *J. Geophys. Res.* 103, 20487–20500. <http://dx.doi.org/10.1029/98JA01740>.
- Thorne, R.M., Horne, R.B., 1997. Modulation of electromagnetic ion cyclotron instability due to interaction with ring current O⁺ during magnetic storms. *J. Geophys. Res.* 102 (A7), 14155–14163.
- Thorne, R.M., Horne, R.B., Jordanova, V.K., Bortnik, J., Glauert, S.A., 2006. Interaction of EMIC waves with thermal plasma and radiation belt particles. In: *Magnetospheric ULF Waves: Synthesis and New Directions*, Geophysical Monograph Series, vol. 169, AGU, Washington, DC, pp. 213–223.
- Van'yan, L.L., Lipatov, A.S., 1974a. Hydromagnetic wave propagation in a three-dimensional magnetosphere. I. *Geomagn. Aeron.* 14 (3), 417–421.
- Van'yan, L.L., A.S. Lipatov, A.S., 1974b. Hydromagnetic wave propagation in a three-dimensional magnetosphere. II. *Geomagn. Aeron.* 14 (5), 714–716.
- Winglee, R.M., 1998. Multi-fluid simulations of the magnetosphere: the identification of the geopause and its variation with IMF. *Geophys. Res. Lett.* 25 (24), 4441–4444.
- Winske, D., Wu, C.S., Li, Y.Y., Mou, Z.Z., Guo, S.Y., 1985. Coupling of newborn ions to the solar wind by electromagnetic instabilities and their interaction with the bow shock. *J. Geophys. Res.* 90, 2713–2726.
- Winske, D., Cowee, M., 2012. Conditions for Debris-Background Ion Interactions and Collisionless Shock Wave Generation. Report, LA-UR-12-22823, July 2.
- Winske, D., Gary, S.P., 2007. Hybrid simulations of debris-ambient ion interactions in astrophysical explosions. *J. Geophys. Res.* 112, A10303. <http://dx.doi.org/10.1029/2007JA012276>.
- Zhang, H., Sibeck, D.G., Zong, Q.-G., McFadden, J.P., Larson, D., Glassmeier, K.-H., Angelopoulos, V., 2012. Global magnetospheric response to an interplanetary shock: THEMIS observations. *Ann. Geophys.* 30, 379–387. <http://dx.doi.org/10.5194/angeo-30-379-2012>.
- Zhu, P., Raeder, J., Germaschewski, K., Hegna, C.C., 2009. Initiation of ballooning instability in the near-Earth plasma sheet prior to the 23 March 2007 THEMIS substorm expansion onset. *Ann. Geophys.* 27 (3), 1129–1138.